

A novel fractional-order hyperchaotic complex system and its synchronization

Mengxin Jin(金孟鑫), Kehui Sun(孙克辉), and Shaobo He(贺少波)
Citation: Chin. Phys. B, 2023, 32 (**6**): 060501. DOI: 10.1088/1674-1056/acc0f6
Journal homepage: http://cpb.iphy.ac.cn; http://iopscience.iop.org/cpb

What follows is a list of articles you may be interested in

Finite-time synchronization of uncertain fractional-order multi-weighted complex networks with external disturbances via adaptive quantized control

Hongwei Zhang(张红伟), Ran Cheng(程然), and Dawei Ding(丁大为)
Chin. Phys. B, 2022, 31 (**10**): 100504. DOI: 10.1088/1674-1056/ac686b

Solutions and memory effect of fractional-order chaotic system: A review

Shaobo He(贺少波), Huihai Wang(王会海), and Kehui Sun(孙克辉)
Chin. Phys. B, 2022, 31 (**6**): 060501. DOI: 10.1088/1674-1056/ac43ae

Transient transition behaviors of fractional-order simplest chaotic circuit with bi-stable locally-active memristor and its ARM-based implementation

Zong-Li Yang(杨宗立), Dong Liang(梁栋), Da-Wei Ding(丁大为), Yong-Bing Hu(胡永兵), and Hao Li(李浩)
Chin. Phys. B, 2021, 30 (**12**): 120515. DOI: 10.1088/1674-1056/ac1fdf

Dynamical analysis, circuit realization, and application in pseudorandom number generators of a fractional-order laser chaotic system

Chenguang Ma(马晨光), Santo Banerjee, Li Xiong(熊丽), Tianming Liu(刘天明), Xintong Han(韩昕彤), and Jun Mou(牟俊)
Chin. Phys. B, 2021, 30 (**12**): 120504. DOI: 10.1088/1674-1056/abfbd4

Adaptive synchronization of a class of fractional-order complex-valued chaotic neural network with time-delay

Mei Li(李梅), Ruo-Xun Zhang(张若洵), and Shi-Ping Yang(杨世平)
Chin. Phys. B, 2021, 30 (**12**): 120503. DOI: 10.1088/1674-1056/abfa09

A novel fractional-order hyperchaotic complex system and its synchronization

Mengxin Jin(金孟鑫), Kehui Sun(孙克辉)†, and Shaobo He(贺少波)

School of Physics and Electronics, Central South University, Changsha 410083, *China*

(Received 8 December 2022; revised manuscript received 21 February 2023; accepted manuscript online 3 March 2023)

A novel fractional-order hyperchaotic complex system is proposed by introducing the Caputo fractional-order derivative operator and a constant term to the complex simplified Lorenz system. The proposed system has different numbers of equilibria for different ranges of parameters. The dynamics of the proposed system is investigated by means of phase portraits, Lyapunov exponents, bifurcation diagrams, and basins of attraction. The results show abundant dynamical characteristics. Particularly, the phenomena of extreme multistability as well as hidden attractors are discovered. In addition, the complex generalized projective synchronization is implemented between two fractional-order hyperchaotic complex systems with different fractional orders. Based on the fractional Lyapunov stability theorem, the synchronization controllers are designed, and the theoretical results are verified and demonstrated by numerical simulations. It lays the foundation for practical applications of the proposed system.

Keywords: fractional calculus, complex hyperchaos, simplified Lorenz system, complex generalized projective synchronization

PACS: 05.45.Jn, 05.45.Pq, 05.45.Xt **DOI:** 10.1088/1674-1056/acc0f6

1. Introduction

Fractional calculus has a history of more than 300 years. Compared with the integer-order calculus, it can describe physical phenomena more accurately. Therefore, with the development of computer science and engineering technology, it becomes an important tool in physics, chemistry, economics, and other fields. At present, there are mainly three methods for the numerical solution of the fractional-order differential equations, *i.e.*, the frequency–domain approximation method,[1] the predictor–corrector method,[2] and the Adomian decomposition method.[3] In terms of time complexity, space complexity, and solution speed, the Adomian decomposition method performs better.[4] So it is widely used to solve fractional-order chaotic systems, and a large number of research results have been obtained.[5–7] For example, Ye *et al.*[8] used the Adomian decomposition method to solve the fractional-order hyperchaotic memristive circuit. Ma *et al.*[9] investigated the fractional-order Hopfield neural network with complex function nonlinear terms. Liu *et al.*[10] constructed and analyzed the fractional-order multi-attribute chaotic system. These research results show that the fractional-order chaotic system has more complicated dynamical characteristics than its integer-order counterpart, and thus it has more practical applications in engineering fields.

In 1982, Fowler *et al.*[11] firstly introduced the complex Lorenz equations. It is the complex extension of the classic Lorenz system. Since then, several other complex chaotic systems have been proposed, such as the complex Chen system,[12] the complex Lü system,[12] the hyperchaotic complex Lorenz system,[13] the hyperchaotic complex Lü system,[14] and so on. In contrast, fractional-order complex chaotic systems have not been actively explored. Dynamics of the fractional-order complex chaotic system and its applications to secure communication and image encryption are investigated in Refs. [15–17]. Since the pioneering work of Pecora and Carroll,[18] the synchronization of chaotic systems has attracted increasing attention among scientists due to its importance and broad applications in science and engineering. In secure communication, the introduction of complex chaotic systems will enhance the content and security of the transmitted information. Therefore, in recent years, many efforts have been devoted to the investigation of the synchronization of complex chaotic systems, and a large number of different types of synchronization schemes have been proposed, such as lag synchronization,[19] complete synchronization,[20] adaptive impulsive synchronization,[21] hybrid modified function projective synchronization,[22] combination complex synchronization,[23] and adaptive complex generalized synchronization.[24] Furthermore, in practical applications, the synchronization of chaotic systems with different fractional orders can provide more flexibility in the selection of systems. To our best knowledge, although the generalized synchronization of the real-variable fractional-order hyperchaotic system has been investigated,[25] the complex generalized projective synchronization of two fractional-order hyperchaotic complex systems with different fractional orders was seldom discussed.

Extreme multistability means that the system has in-

†Corresponding author. E-mail: kehui@csu.edu.cn

© 2023 Chinese Physical Society and IOP Publishing Ltd

finitely many coexisting attractors.[26] Recently, the extreme multistability in nonlinear dynamical systems has become an important research topic, and it has been discovered in some memristive circuits and systems.[27–29] For example, Bao *et al.*[30] proposed a non-autonomous memristor-based FitzHugh–Nagumo circuit with extreme multistability. Chang *et al.*[31] established and investigated a simplest memristor-based circuit as a quasi-Hamiltonian system with extreme multistability. Yuan *et al.*[32] reported the phenomenon of extreme multistability in a memristor-based multi-scroll hyperchaotic system. In addition, the investigation of hidden attractors in dynamical systems has attracted much attention in recent years. An attractor is called the hidden attractor if its basin of attraction does not intersect with small neighborhoods of equilibria,[33] and it usually exists in dynamical systems with no equilibrium. Currently, many no-equilibrium systems that can yield hidden attractors have been reported. For example, Wei[34] proposed a simple three-dimensional (3D) system with no equilibrium by introducing a tiny perturbation to the Sprott D system. Pham *et al.*[35] constructed a new no-equilibrium chaotic system by adding a tiny perturbation to a simple chaotic flow. Lai *et al.*[36] presented a novel four-dimensional (4D) no-equilibrium system with hidden attractors and coexisting attractors. However, all the above-mentioned dynamical systems are real-variable dynamical systems. In contrast, the extreme multistability and hidden attractors in complex-variable dynamical systems have rarely been reported.

In this paper, we focus on the numerical solution, dynamical behaviors, and synchronization of a novel fractional-order hyperchaotic complex system. The rest of this paper is organized as follows. In Section 2, the novel fractional-order hyperchaotic complex system is proposed and numerically solved. In Section 3, the dynamics of the proposed system is analyzed. In Section 4, the complex generalized projective synchronization of two fractional-order hyperchaotic complex systems with different fractional orders is investigated, and the numerical simulations are performed to illustrate the correctness of the theoretical results. Finally, the results of this paper are summarized and the future directions are indicated.

2. The novel fractional-order hyperchaotic complex system and its solution

2.1. Model of the fractional-order hyperchaotic complex simplified Lorenz system

In 2009, Sun and Sprott[37] proposed the simplified Lorenz system with a single adjustable parameter c, which is described by

$$\begin{cases} \dot{x} = 10(y-x), \\ \dot{y} = (24-4c)x + cy - xz, \\ \dot{z} = -8/3z + xy, \end{cases} \tag{1}$$

where $x, y, z \in \mathbb{R}$ are state variables. When $c \in [-1.59, 7.75]$, system (1) exhibits typical chaotic behaviors. Later, in 2021, by extending the state variables x, y from real domain to complex domain, we proposed the complex simplified Lorenz system,[38] which is depicted as

$$\begin{cases} \dot{x} = 10(y-x), \\ \dot{y} = (24-4c)x + cy - xz, \\ \dot{z} = -8/3z + 1/2(\bar{x}y + x\bar{y}), \end{cases} \tag{2}$$

where $x, y \in \mathbb{C}$ are complex state variables. $z \in \mathbb{R}$ is a real state variable, and $\bar{x}, \bar{y}$ stand for the complex conjugate variables of x, y, respectively. Here, by introducing the Caputo fractional-order derivative operator and a constant term to system (2), the fractional-order hyperchaotic complex simplified Lorenz system is obtained as

$$\begin{cases} D_{t_0}^q x = 10(y-x), \\ D_{t_0}^q y = (24-4c)x + cy - xz + k, \\ D_{t_0}^q z = -8/3z + 1/2(\bar{x}y + x\bar{y}), \end{cases} \tag{3}$$

where $D_{t_0}^q$ is the Caputo fractional-order derivative operator of order q. $x, y \in \mathbb{C}$ are complex state variables. $z \in \mathbb{R}$ is a real state variable, and $c, k \in \mathbb{R}$ are the system parameters. Because of the linearity of $D_{t_0}^q$, let $x = u_1 + \mathrm{j}u_2$, $y = u_3 + \mathrm{j}u_4$, $z = u_5$, where $\mathrm{j} = \sqrt{-1}$, then system (3) can be rewritten as a real-variable system

$$\begin{cases} D_{t_0}^q u_1 = 10(u_3 - u_1), \\ D_{t_0}^q u_2 = 10(u_4 - u_2), \\ D_{t_0}^q u_3 = (24-4c)u_1 + cu_3 - u_1u_5 + k, \\ D_{t_0}^q u_4 = (24-4c)u_2 + cu_4 - u_2u_5, \\ D_{t_0}^q u_5 = -8/3u_5 + u_1u_3 + u_2u_4, \end{cases} \tag{4}$$

where $u_1, u_2, u_3, u_4, u_5 \in \mathbb{R}$ are real state variables.

2.2. Adomian decomposition method

Definition 1 The Riemann–Liouville fractional-order integration is defined as

$$J_{t_0}^q x(t) = \frac{1}{\Gamma(q)} \int_{t_0}^{t} (t-\tau)^{q-1} x(\tau) \mathrm{d}\tau, \tag{5}$$

where $J_{t_0}^q$ represents the Riemann–Liouville fractional-order integral operator. When $t \in [t_0, t_1]$, $q \geq 0$, $\gamma \geq -1$, $r \geq 0$, and C is a real constant, we have

$$J_{t_0}^q (t-t_0)^\gamma = \frac{\Gamma(\gamma+1)}{\Gamma(\gamma+1+q)} (t-t_0)^{\gamma+q}, \tag{6}$$

$$J_{t_0}^q C = \frac{C}{\Gamma(q+1)} (t-t_0)^q, \tag{7}$$

$$J_{t_0}^q J_{t_0}^r x(t) = J_{t_0}^{q+r} x(t). \tag{8}$$

The n-dimensional fractional-order chaotic system is divided into three terms

$$D_{t_0}^q x(t) = Lx(t) + Nx(t) + g(t), \tag{9}$$

where $Lx(t)$ and $Nx(t)$ represent the linear and nonlinear terms of the fractional-order chaotic system, respectively. $g(t) = [g_1(t), g_2(t), \ldots, g_n(t)]$ are constants. The initial condition is given as $x^{(\sigma)}(t_0^+) = b_\sigma$, $\sigma = 0, 1, \ldots, m-1$, $m \in \mathbb{N}$, $m-1 < q \leq m$. By applying the fractional-order integral operator $J_{t_0}^q$ to both sides of Eq. (9), we obtain

$$x = J_{t_0}^q Lx + J_{t_0}^q Nx + J_{t_0}^q g + \sum_{\sigma=0}^{m-1} b_\sigma \frac{(t-t_0)^\sigma}{\sigma!}. \tag{10}$$

The nonlinear term of Eq. (9) is decomposed by

$$\begin{cases} A_j^i = \dfrac{1}{i!}\left[\dfrac{\mathrm{d}^i}{\mathrm{d}\lambda^i} N(v_j^i(\lambda))\right]_{\lambda=0}, \\ v_j^i(\lambda) = \displaystyle\sum_{\sigma=0}^{i} (\lambda)^\sigma x_j^\sigma, \end{cases} \tag{11}$$

where $i = 0, 1, 2, \ldots, \infty$ and $j = 1, 2, \ldots, n$. The nonlinear term is expressed as

$$Nx = \sum_{i=0}^{\infty} A^i(x^0, x^1, \cdots, x^i). \tag{12}$$

Therefore, the numerical solution of Eq. (9) is obtained as

$$x = \sum_{i=0}^{\infty} x^i = J_{t_0}^q \sum_{i=0}^{\infty} Lx^i + J_{t_0}^q \sum_{i=0}^{\infty} A^i + J_{t_0}^q g + \sum_{\sigma=0}^{m-1} b_\sigma \frac{(t-t_0)^\sigma}{\sigma!}, \tag{13}$$

where $x^0, x^1, x^2, \ldots, x^i, \ldots$ are calculated by

$$\begin{cases} x^0 = J_{t_0}^q g + \displaystyle\sum_{\sigma=0}^{m-1} b_\sigma \frac{(t-t_0)^\sigma}{\sigma!}, \\ x^1 = J_{t_0}^q Lx^0 + J_{t_0}^q A^0(x^0), \\ x^2 = J_{t_0}^q Lx^1 + J_{t_0}^q A^1(x^0, x^1), \\ \quad \ldots \\ x^i = J_{t_0}^q Lx^{i-1} + J_{t_0}^q A^{i-1}(x^0, x^1, \cdots, x^{i-1}), \\ \quad \ldots \end{cases} \tag{14}$$

2.3. Solution of the fractional-order hyperchaotic complex simplified Lorenz system

In this part, the Adomian decomposition method is applied to solve the fractional-order hyperchaotic complex simplified Lorenz system. Firstly, the system is divided into three terms according to Eq. (9), *i.e.*,

$$\begin{bmatrix} L_{u_1} \\ L_{u_2} \\ L_{u_3} \\ L_{u_4} \\ L_{u_5} \end{bmatrix} = \begin{bmatrix} 10(u_3 - u_1) \\ 10(u_4 - u_2) \\ (24-4c)u_1 + cu_3 \\ (24-4c)u_2 + cu_4 \\ -8/3u_5 \end{bmatrix}, \quad \begin{bmatrix} N_{u_1} \\ N_{u_2} \\ N_{u_3} \\ N_{u_4} \\ N_{u_5} \end{bmatrix} = \begin{bmatrix} 0 \\ 0 \\ -u_1 u_5 \\ -u_2 u_5 \\ u_1 u_3 + u_2 u_4 \end{bmatrix}, \quad \begin{bmatrix} g_1 \\ g_2 \\ g_3 \\ g_4 \\ g_5 \end{bmatrix} = \begin{bmatrix} 0 \\ 0 \\ k \\ 0 \\ 0 \end{bmatrix}. \tag{15}$$

Considering the fast convergence of the Adomian decomposition method, the first five terms of the series are truncated for the solution of the system. $A_3 = -u_1 u_5$, $A_4 = -u_2 u_5$, $A_5 = u_1 u_3 + u_2 u_4$ are the three nonlinear terms of the system, which are decomposed by

$$\begin{aligned} A_3^0 &= -u_1^0 u_5^0, \quad A_3^1 = -u_1^1 u_5^0 - u_1^0 u_5^1, \\ A_3^2 &= -u_1^2 u_5^0 - u_1^1 u_5^1 - u_1^0 u_5^2, \\ A_3^3 &= -u_1^3 u_5^0 - u_1^2 u_5^1 - u_1^1 u_5^2 - u_1^0 u_5^3, \end{aligned} \tag{16}$$

$$\begin{aligned} A_4^0 &= -u_2^0 u_5^0, \quad A_4^1 = -u_2^1 u_5^0 - u_2^0 u_5^1, \\ A_4^2 &= -u_2^2 u_5^0 - u_2^1 u_5^1 - u_2^0 u_5^2, \\ A_4^3 &= -u_2^3 u_5^0 - u_2^2 u_5^1 - u_2^1 u_5^2 - u_2^0 u_5^3, \end{aligned} \tag{17}$$

$$\begin{aligned} A_5^0 &= u_1^0 u_3^0 + u_2^0 u_4^0, \\ A_5^1 &= u_1^1 u_3^0 + u_1^0 u_3^1 + u_2^1 u_4^0 + u_2^0 u_4^1, \\ A_5^2 &= u_1^2 u_3^0 + u_1^1 u_3^1 + u_1^0 u_3^2 + u_2^2 u_4^0 + u_2^1 u_4^1 + u_2^0 u_4^2, \\ A_5^3 &= u_1^3 u_3^0 + u_1^2 u_3^1 + u_1^1 u_3^2 + u_1^0 u_3^3 + u_2^3 u_4^0 + u_2^2 u_4^1 \\ &\quad + u_2^1 u_4^2 + u_2^0 u_4^3. \end{aligned} \tag{18}$$

According to the initial condition, the first term is obtained as

$$u_1^0 = u_1(t_0), \quad u_2^0 = u_2(t_0),$$

$$u_3^0 = u_3(t_0) + k\frac{(t-t_0)^q}{\Gamma(q+1)}, \quad u_4^0 = u_4(t_0), \quad u_5^0 = u_5(t_0). \tag{19}$$

Let $c_1^0 = u_1^0 = u_1(t_0)$, $c_2^0 = u_2^0 = u_2(t_0)$, $c_3^0 = u_3(t_0)$, $c_4^0 = u_4^0 = u_4(t_0)$, $c_5^0 = u_5^0 = u_5(t_0)$, and the second term is calculated by

$$\begin{aligned} u_1^1 &= c_1^1 \frac{(t-t_0)^q}{\Gamma(q+1)} + c_1^{10} \frac{(t-t_0)^{2q}}{\Gamma(2q+1)}, \\ u_2^1 &= c_2^1 \frac{(t-t_0)^q}{\Gamma(q+1)}, \\ u_3^1 &= c_3^1 \frac{(t-t_0)^q}{\Gamma(q+1)} + c_3^{10} \frac{(t-t_0)^{2q}}{\Gamma(2q+1)}, \\ u_4^1 &= c_4^1 \frac{(t-t_0)^q}{\Gamma(q+1)}, \\ u_5^1 &= c_5^1 \frac{(t-t_0)^q}{\Gamma(q+1)} + c_5^{10} \frac{(t-t_0)^{2q}}{\Gamma(2q+1)}, \end{aligned} \tag{20}$$

where

$$\begin{aligned} &c_1^1 = 10(c_3^0 - c_1^0), \quad c_1^{10} = 10k, \quad c_2^1 = 10(c_4^0 - c_2^0), \\ &c_3^1 = (24-4c)c_1^0 + cc_3^0 - c_1^0 c_5^0, \\ &c_3^{10} = ck, \quad c_4^1 = (24-4c)c_2^0 + cc_4^0 - c_2^0 c_5^0, \end{aligned}$$

$$c_5^1=-8/3c_5^0+c_1^0c_3^0+c_2^0c_4^0,\quad c_5^{10}=kc_1^0. \tag{21}$$

Similarly, the third term is calculated by

$$\begin{aligned}
u_1^2&=c_1^2\frac{(t-t_0)^{2q}}{\Gamma(2q+1)}+c_1^{20}\frac{(t-t_0)^{3q}}{\Gamma(3q+1)},\\
u_2^2&=c_2^2\frac{(t-t_0)^{2q}}{\Gamma(2q+1)},\\
u_3^2&=c_3^2\frac{(t-t_0)^{2q}}{\Gamma(2q+1)}+c_3^{20}\frac{(t-t_0)^{3q}}{\Gamma(3q+1)},\\
u_4^2&=c_4^2\frac{(t-t_0)^{2q}}{\Gamma(2q+1)}+c_4^{20}\frac{(t-t_0)^{3q}}{\Gamma(3q+1)},\\
u_5^2&=c_5^2\frac{(t-t_0)^{2q}}{\Gamma(2q+1)}+c_5^{20}\frac{(t-t_0)^{3q}}{\Gamma(3q+1)}+c_5^{21}\frac{(t-t_0)^{4q}}{\Gamma(4q+1)},
\end{aligned} \tag{22}$$

where

$$\begin{aligned}
&c_1^2=10(c_3^1-c_1^1),\ \ c_1^{20}=10(c_3^{10}-c_1^{10}),\ \ c_2^2=10(c_4^1-c_2^1),\\
&c_3^2=(24-4c)c_1^1+cc_3^1-c_1^1c_5^0-c_1^0c_5^1,\\
&c_3^{20}=(24-4c)c_1^{10}+cc_3^{10}-c_1^{10}c_5^0-c_1^0c_5^{10},\\
&c_4^2=(24-4c)c_2^1+cc_4^1-c_2^1c_5^0-c_2^0c_5^1,\ \ c_4^{20}=-c_2^0c_5^{10},\\
&c_5^2=-8/3c_5^1+c_1^1c_3^0+c_1^0c_3^1+c_2^1c_4^0+c_2^0c_4^1,\\
&c_5^{20}=-8/3c_5^{10}+c_1^{10}c_3^0+c_1^0c_3^{10}+kc_1^1\frac{\Gamma(2q+1)}{\Gamma^2(q+1)},\\
&c_5^{21}=kc_1^{10}\frac{\Gamma(3q+1)}{\Gamma(q+1)\Gamma(2q+1)}.
\end{aligned} \tag{23}$$

The fourth term is calculated by

$$\begin{aligned}
u_1^3&=c_1^3\frac{(t-t_0)^{3q}}{\Gamma(3q+1)}+c_1^{30}\frac{(t-t_0)^{4q}}{\Gamma(4q+1)},\\
u_2^3&=c_2^3\frac{(t-t_0)^{3q}}{\Gamma(3q+1)}+c_2^{30}\frac{(t-t_0)^{4q}}{\Gamma(4q+1)},\\
u_3^3&=c_3^3\frac{(t-t_0)^{3q}}{\Gamma(3q+1)}+c_3^{30}\frac{(t-t_0)^{4q}}{\Gamma(4q+1)}+c_3^{31}\frac{(t-t_0)^{5q}}{\Gamma(5q+1)},\\
u_4^3&=c_4^3\frac{(t-t_0)^{3q}}{\Gamma(3q+1)}+c_4^{30}\frac{(t-t_0)^{4q}}{\Gamma(4q+1)}+c_4^{31}\frac{(t-t_0)^{5q}}{\Gamma(5q+1)},\\
u_5^3&=c_5^3\frac{(t-t_0)^{3q}}{\Gamma(3q+1)}+c_5^{30}\frac{(t-t_0)^{4q}}{\Gamma(4q+1)}+c_5^{31}\frac{(t-t_0)^{5q}}{\Gamma(5q+1)},
\end{aligned} \tag{24}$$

where

$$\begin{aligned}
&c_1^3=10(c_3^2-c_1^2),\ \ c_1^{30}=10(c_3^{20}-c_1^{20}),\ \ c_2^3=10(c_4^2-c_2^2),\\
&c_2^{30}=10c_4^{20},\\
&c_3^3=(24-4c)c_1^2+cc_3^2-c_1^2c_5^0-c_1^1c_5^1\frac{\Gamma(2q+1)}{\Gamma^2(q+1)}-c_1^0c_5^2,\\
&c_3^{30}=(24-4c)c_1^{20}+cc_3^{20}-c_1^{20}c_5^0\\
&\qquad-(c_1^1c_5^{10}+c_1^{10}c_5^1)\frac{\Gamma(3q+1)}{\Gamma(q+1)\Gamma(2q+1)}-c_1^0c_5^{20},\\
&c_3^{31}=-c_1^0c_5^{21}-c_1^{10}c_5^{10}\frac{\Gamma(4q+1)}{\Gamma^2(2q+1)},\\
&c_4^3=(24-4c)c_2^2+cc_4^2-c_2^2c_5^0-c_2^1c_5^1\frac{\Gamma(2q+1)}{\Gamma^2(q+1)}-c_2^0c_5^2,\\
&c_4^{30}=cc_4^{20}-c_2^0c_5^{20}-c_2^1c_5^{10}\frac{\Gamma(3q+1)}{\Gamma(q+1)\Gamma(2q+1)},\\
&c_4^{31}=-c_2^0c_5^{21},\\
&c_5^3=-8/3c_5^2+c_1^2c_3^0+c_1^0c_3^2+c_2^2c_4^0+c_2^0c_4^2+(c_1^1c_3^1\\
&\qquad+c_2^1c_4^1)\frac{\Gamma(2q+1)}{\Gamma^2(q+1)},\\
&c_5^{30}=-8/3c_5^{20}+c_1^{20}c_3^0+c_1^0c_3^{20}+c_2^0c_4^{20}\\
&\qquad+(kc_1^2+c_1^1c_3^{10}+c_1^{10}c_3^1)\frac{\Gamma(3q+1)}{\Gamma(q+1)\Gamma(2q+1)},\\
&c_5^{31}=-8/3c_5^{21}+c_1^{10}c_3^{10}\frac{\Gamma(4q+1)}{\Gamma^2(2q+1)}\\
&\qquad+kc_1^{20}\frac{\Gamma(4q+1)}{\Gamma(q+1)\Gamma(3q+1)}.
\end{aligned} \tag{25}$$

Finally, the fifth term is calculated by

$$\begin{aligned}
u_1^4&=c_1^4\frac{(t-t_0)^{4q}}{\Gamma(4q+1)}+c_1^{40}\frac{(t-t_0)^{5q}}{\Gamma(5q+1)}+c_1^{41}\frac{(t-t_0)^{6q}}{\Gamma(6q+1)},\\
u_2^4&=c_2^4\frac{(t-t_0)^{4q}}{\Gamma(4q+1)}+c_2^{40}\frac{(t-t_0)^{5q}}{\Gamma(5q+1)}+c_2^{41}\frac{(t-t_0)^{6q}}{\Gamma(6q+1)},\\
u_3^4&=c_3^4\frac{(t-t_0)^{4q}}{\Gamma(4q+1)}+c_3^{40}\frac{(t-t_0)^{5q}}{\Gamma(5q+1)}+c_3^{41}\frac{(t-t_0)^{6q}}{\Gamma(6q+1)}\\
&\quad+c_3^{42}\frac{(t-t_0)^{7q}}{\Gamma(7q+1)},\\
u_4^4&=c_4^4\frac{(t-t_0)^{4q}}{\Gamma(4q+1)}+c_4^{40}\frac{(t-t_0)^{5q}}{\Gamma(5q+1)}+c_4^{41}\frac{(t-t_0)^{6q}}{\Gamma(6q+1)},\\
u_5^4&=c_5^4\frac{(t-t_0)^{4q}}{\Gamma(4q+1)}+c_5^{40}\frac{(t-t_0)^{5q}}{\Gamma(5q+1)}+c_5^{41}\frac{(t-t_0)^{6q}}{\Gamma(6q+1)},
\end{aligned} \tag{26}$$

where

$$\begin{aligned}
&c_1^4=10(c_3^3-c_1^3),\ \ c_1^{40}=10(c_3^{30}-c_1^{30}),\ \ c_1^{41}=10c_3^{31},\\
&c_2^4=10(c_4^3-c_2^3),\ \ c_2^{40}=10(c_4^{30}-c_2^{30}),\ \ c_2^{41}=10c_4^{31},\\
&c_3^4=(24-4c)c_1^3+cc_3^3-c_1^3c_5^0\\
&\qquad-(c_1^2c_5^1+c_1^1c_5^2)\frac{\Gamma(3q+1)}{\Gamma(q+1)\Gamma(2q+1)}-c_1^0c_5^3,\\
&c_3^{40}=(24-4c)c_1^{30}+cc_3^{30}-c_1^{30}c_5^0-c_1^0c_5^{30}\\
&\qquad-(c_1^2c_5^{10}+c_1^{10}c_5^2)\frac{\Gamma(4q+1)}{\Gamma^2(2q+1)}\\
&\qquad-(c_1^{20}c_5^1+c_1^1c_5^{20})\frac{\Gamma(4q+1)}{\Gamma(q+1)\Gamma(3q+1)},\\
&c_3^{41}=cc_3^{31}-c_1^0c_5^{31}-c_1^1c_5^{21}\frac{\Gamma(5q+1)}{\Gamma(q+1)\Gamma(4q+1)}\\
&\qquad-(c_1^{20}c_5^{10}+c_1^{10}c_5^{20})\frac{\Gamma(5q+1)}{\Gamma(2q+1)\Gamma(3q+1)},\\
&c_3^{42}=-c_1^{10}c_5^{21}\frac{\Gamma(6q+1)}{\Gamma(2q+1)\Gamma(4q+1)},\\
&c_4^4=(24-4c)c_2^3+cc_4^3-c_2^3c_5^0
\end{aligned}$$

$$
\begin{aligned}
&- (c_2^2c_5^1 + c_2^1c_5^2)\frac{\Gamma(3q+1)}{\Gamma(q+1)\Gamma(2q+1)} - c_2^0c_5^3,\\
c_4^{40} &= (24-4c)c_2^{30} + cc_4^{30} - c_2^{30}c_5^0 - c_2^0c_5^{30}\\
&\quad - c_2^2c_5^{10}\frac{\Gamma(4q+1)}{\Gamma^2(2q+1)} - c_2^1c_5^{20}\frac{\Gamma(4q+1)}{\Gamma(q+1)\Gamma(3q+1)},\\
c_4^{41} &= cc_4^{31} - c_2^0c_5^{31} - c_2^1c_5^{21}\frac{\Gamma(5q+1)}{\Gamma(q+1)\Gamma(4q+1)},\\
c_5^4 &= -8/3c_5^3 + c_1^3c_3^0 + c_1^0c_3^3 + c_2^3c_4^0 + c_2^0c_4^3\\
&\quad + (c_1^2c_3^1 + c_1^1c_3^2 + c_2^2c_4^1 + c_2^1c_4^2)\frac{\Gamma(3q+1)}{\Gamma(q+1)\Gamma(2q+1)},\\
c_5^{40} &= -8/3c_5^{30} + c_1^{30}c_3^0 + c_1^0c_3^{30} + c_2^{30}c_4^0 + c_2^0c_4^{30}\\
&\quad + (c_1^2c_3^{10} + c_1^{10}c_3^2)\frac{\Gamma(4q+1)}{\Gamma^2(2q+1)}\\
&\quad + (kc_1^3 + c_1^{20}c_3^1 + c_1^1c_3^{20} + c_2^1c_4^{20})\frac{\Gamma(4q+1)}{\Gamma(q+1)\Gamma(3q+1)},\\
c_5^{41} &= -8/3c_5^{31} + c_1^0c_3^{31} + c_2^0c_4^{31} + kc_1^{30}\frac{\Gamma(5q+1)}{\Gamma(q+1)\Gamma(4q+1)}\\
&\quad + (c_1^{20}c_3^{10} + c_1^{10}c_3^{20})\frac{\Gamma(5q+1)}{\Gamma(2q+1)\Gamma(3q+1)}.
\end{aligned}
\tag{27}
$$

Therefore, the numerical solution of the system is obtained as follows:

$$
\begin{bmatrix}\tilde{u}_1(t)\\ \tilde{u}_2(t)\\ \tilde{u}_3(t)\\ \tilde{u}_4(t)\\ \tilde{u}_5(t)\end{bmatrix} = \begin{bmatrix}u_1^0(t)+u_1^1(t)+u_1^2(t)+u_1^3(t)+u_1^4(t)\\ u_2^0(t)+u_2^1(t)+u_2^2(t)+u_2^3(t)+u_2^4(t)\\ u_3^0(t)+u_3^1(t)+u_3^2(t)+u_3^3(t)+u_3^4(t)\\ u_4^0(t)+u_4^1(t)+u_4^2(t)+u_4^3(t)+u_4^4(t)\\ u_5^0(t)+u_5^1(t)+u_5^2(t)+u_5^3(t)+u_5^4(t)\end{bmatrix}. \tag{28}
$$

3. Dynamical analysis

3.1. Symmetry and stability

When the parameter $k = 0$, system (4) has rotational symmetry about the u_5 axis, *i.e.*, the system is symmetric and invariant under the coordinates transformation: $(u_1,u_2,u_3,u_4,u_5) \to (-u_1,-u_2,-u_3,-u_4,u_5)$. Moreover, this symmetry exists for any choice of the parameter c.

Next, we turn to investigate the equilibria of system (4), which can be obtained by solving the following nonlinear equations:

$$
\begin{aligned}
&10(u_3-u_1) = 0, \quad 10(u_4-u_2) = 0,\\
&(24-4c)u_1 + cu_3 - u_1u_5 + k = 0,\\
&(24-4c)u_2 + cu_4 - u_2u_5 = 0,\\
&-8/3u_5 + u_1u_3 + u_2u_4 = 0.
\end{aligned}
\tag{29}
$$

Obviously, system (4) has different numbers of equilibria for different ranges of the parameters. If $k \neq 0$, then system (4) has no equilibrium, which implies that the attractors generated are all hidden. If $k = 0$, then system (4) always has one equilibrium, *i.e.*, the origin $E_0 = (0,0,0,0,0)$. Particularly, when $c < 8$, system (4) has infinite circular equilibria, which are expressed as

$$
E_\theta = \left(r\cos\theta, r\sin\theta, r\cos\theta, r\sin\theta, \frac{3}{8}r^2\right), \tag{30}
$$

where $r = \sqrt{64-8c}$, and $\theta \in [0, 2\pi]$. The stability of E_0 can be obtained through the Jacobian matrix of system (4) at E_0, which is written as

$$
J_0 = \begin{bmatrix}-10 & 0 & 10 & 0 & 0\\ 0 & -10 & 0 & 10 & 0\\ 24-4c & 0 & c & 0 & 0\\ 0 & 24-4c & 0 & c & 0\\ 0 & 0 & 0 & 0 & -8/3\end{bmatrix}, \tag{31}
$$

and its eigenvalue μ satisfies

$$
\left(\mu + \frac{8}{3}\right)\left[\mu^2 + (10-c)\mu + 30c - 240\right]^2 = 0, \tag{32}
$$

thus we have

$$
\mu_1 = -\frac{8}{3}, \quad \mu_2 = \mu_3 = \alpha + \mathrm{j}\beta, \quad \mu_4 = \mu_5 = \alpha - \mathrm{j}\beta, \tag{33}
$$

where

$$
\alpha = \frac{c-10}{2}, \quad \beta = \frac{\sqrt{-c^2+140c-1060}}{2}. \tag{34}
$$

Therefore, according to the stability theory of fractional-order systems,[39] if the inequality

$$
q > \frac{2}{\pi}\arctan\left(\frac{|\beta|}{\alpha}\right)
$$

holds, then E_0 is stable, otherwise it is unstable. Similarly, the stability of E_θ can be obtained through the Jacobian matrix of system (4) at E_θ, which is written as

$$
J_\theta = \begin{bmatrix}-10 & 0 & 10 & 0 & 0\\ 0 & -10 & 0 & 10 & 0\\ -c & 0 & c & 0 & -r\cos\theta\\ 0 & -c & 0 & c & -r\sin\theta\\ r\cos\theta & r\sin\theta & r\cos\theta & r\sin\theta & -8/3\end{bmatrix}, \tag{35}
$$

and its eigenvalue μ satisfies

$$
\begin{aligned}
&\mu(\mu+10-c)\left[\mu^3 + \left(\frac{38}{3}-c\right)\mu^2\right.\\
&\left.+\left(r^2 + \frac{80}{3} - \frac{8}{3}c\right)\mu + 20r^2\right] = 0,
\end{aligned}
\tag{36}
$$

thus we have

$$
\mu_1 = 0, \quad \mu_2 = c - 10,
$$

and according to the Routh–Hurwitz criterion, system (4) has a negative real eigenvalue and a pair of conjugate complex eigenvalues with positive real parts provided $c \in [-1.59, 7.75]$. Let

$$
\mu_3 = -\rho, \quad \mu_4 = \omega + \mathrm{j}\varphi, \quad \mu_5 = \omega - \mathrm{j}\varphi,
$$

where ρ, ω, φ are positive real numbers. According to the stability theory of fractional-order systems, if the inequality

$$
q > \frac{2}{\pi}\arctan\left(\frac{|\varphi|}{\omega}\right)
$$

holds, then E_θ is stable, otherwise it is unstable.

3.2. Bifurcation and chaos with different fractional orders and system parameters

The bifurcation diagram and Lyapunov exponent spectrum are important indexes to measure the dynamical behaviors of a nonlinear system. Here, the QR decomposition method[40] is applied to calculate the Lyapunov exponents of the system. Dynamics of system (4) with different fractional orders and system parameters is discussed in the following three cases.

(i) Fix $c = 5$, $k = 0$, and the initial condition is selected as $u_0 = (1,-1,1,-1,1)$. q varies at the range $[0.5,1]$ with an increment of $\Delta q = 0.005$. The bifurcation diagram and Lyapunov exponents of system (4) are shown in Fig. 1.

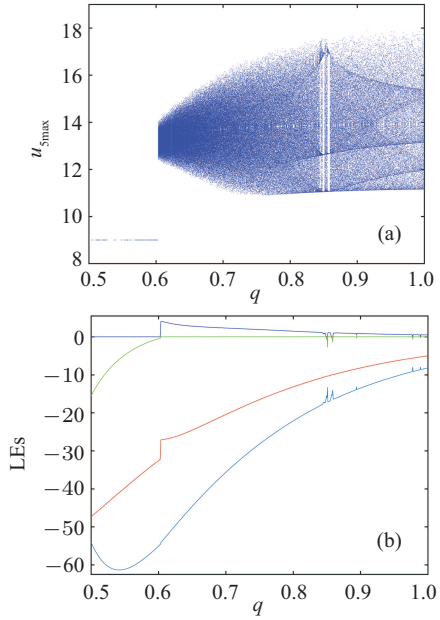


Fig. 1. Dynamics of system (4) with q varying: (a) bifurcation diagram and (b) Lyapunov exponents.

The figure shows that system (4) is chaotic over most of the range $q \in [0.604,1]$. Therefore, the minimum value of q to generate chaos is 0.604. In addition, when q decreases from 1 to 0.604, the maximum Lyapunov exponent of system (4) increases. It illustrates that the fractional-order system is more complicated than its integer-order counterpart. The figure also shows that when q increases from 0.5 to 0.604, system (4) enters into chaos abruptly at $q \cong 0.604$. Moreover, some periodic windows are observed in the range $[0.8,1]$, such as $W_1 = [0.849,0.851]$, and $W_2 = [0.857,0.859]$. In particular, suppose that $q = 0.95$, $c = 5$, and $k = 0$, then all the five Lyapunov exponents of system (4) are calculated as $\lambda_1 = 0.6600$, $\lambda_2 = 0$, $\lambda_3 = 0$, $\lambda_4 = -6.4081$, and $\lambda_5 = -10.5096$. Hence, the corresponding Lyapunov dimension of system (4) is obtained as

$$D_{\mathrm{L}} = l + \frac{1}{|\lambda_{l+1}|}\sum_{n=1}^{l}\lambda_n = 3 + \frac{0.6600}{|-6.4081|} = 3.1030, \quad (37)$$

where l is the largest integer that satisfies $\sum_{n=1}^{l}\lambda_n > 0$ and $\sum_{n=1}^{l+1}\lambda_n < 0$. Because of the fractional Lyapunov dimension and positive Lyapunov exponent, system (4) is chaotic in this case. Furthermore, the phase portrait of system (4) is plotted in Fig. 2(a), and its corresponding Poincaré section generated on the hyperplane $u_5 = 9$ is plotted in Fig. 2(b). Obviously, there exists a typical double-scroll chaotic attractor.

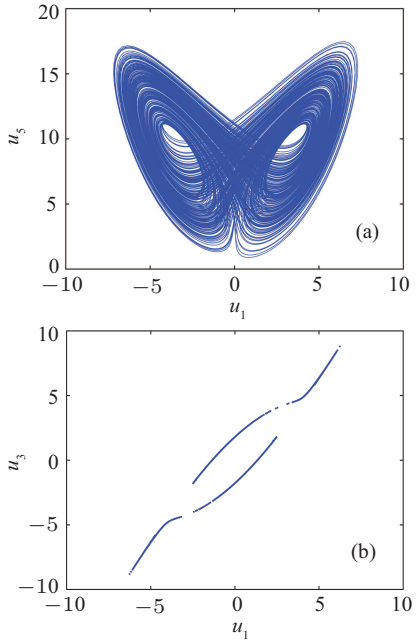


Fig. 2. Phase portrait and Poincaré section of system (4) for $q = 0.95$, $c = 5$, $k = 0$: (a) phase portrait and (b) Poincaré section.

To demonstrate the correctness of the lowest order that yields chaos, we apply the 0–1 test[41] to determine the underlying dynamical state of system (4). The one-dimensional discrete sequence $\phi(n)$ $(n = 1,2,3,\ldots)$ obtained from the iterative formula (28) is selected for the 0–1 test. Two equations are defined by

$$\begin{cases} p(n) = \sum_{j=1}^{n}\phi(j)\cos(\theta(j)), \\ s(n) = \sum_{j=1}^{n}\phi(j)\sin(\theta(j)), \end{cases} \quad (38)$$

where

$$\theta(j) = j\delta + \sum_{i=1}^{j}\phi(i), \quad (39)$$

and $\delta \in \mathbb{R}^+$ is an arbitrary positive constant. The trajectories are plotted on the (p,s)-plane. If the trajectories are bounded, then the system is convergent or periodic, whereas the Brownian-like trajectories indicate that the underlying dynamical state of the system is chaotic. Figure 3 shows the trajectories plotted on the (p,s)-plane when $q = 0.603$, and $q = 0.604$, respectively. The figure illustrates that the system (4) is convergent when $q = 0.603$, and it is chaotic when $q = 0.604$. Therefore, the lowest order of the system (4) that yields chaoic state is $3 \times 0.604 = 1.812$.

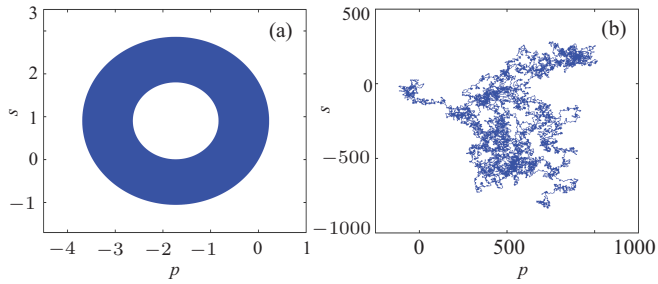


Fig. 3. The (p,s)-plane of system (4) for $c=5$, $k=0$: (a) $q=0.603$ and (b) $q=0.604$.

(ii) Fix $q=0.95$, $k=3.5$, and the initial condition keeps the same as above. c varies at the range $[-2,8]$ with an increment of $\Delta c=0.01$. In this case, all the attractors of system (4) are hidden attractors since the system has no equilibrium. The bifurcation diagram and Lyapunov exponents of system (4) are shown in Fig. 4. The figure shows that system (4) is hyperchaotic over most of the range $c\in[1,5]$, and is chaotic in most of the range $c\in[-1.06,1]\cup[5,7.07]$. In particular, system (4) is quasi-periodic over the range $c\in[7.10,7.18]$. The figure also shows that when c increases from $-\infty$ to -1.06, system (4) enters into chaos abruptly at $c\cong-1.06$ by a boundary crisis bifurcation. When c increases further, system (4) degenerates from chaos to periodic state through the quasi-periodic state. Moreover, the phase portraits of system (4) for different system parameter c are shown in Fig. 5. Obviously, system (4) has four different types of hidden attractors, which displays its complicated dynamical characteristics.

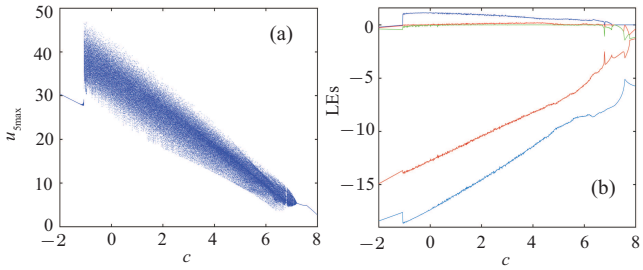


Fig. 4. Dynamics of system (4) with c varying: (a) bifurcation diagram and (b) Lyapunov exponents.

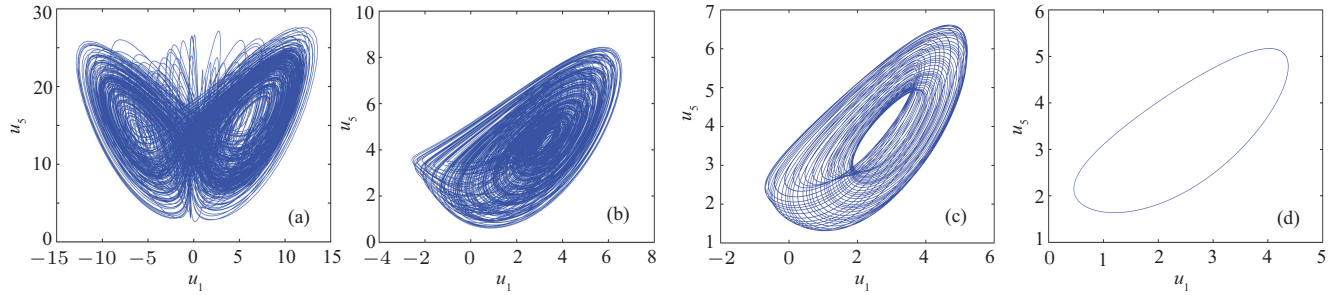


Fig. 5. Hidden attractors of system (4) for $q=0.95$, $k=3.5$ with different system parameter c: (a) $c=3$ (hyperchaotic), (b) $c=6.9$ (chaotic), (c) $c=7.1$ (quasi-periodic), and (d) $c=7.3$ (periodic).

(iii) Fix $q=0.95$, $c=2.5$, and the initial condition keeps unchanged. Parameter k varies at the range $[-25,25]$ with an increment of $\Delta k=0.05$. The bifurcation diagram and Lyapunov exponents of system (4) are shown in Fig. 6. The figure shows that system (4) is hyperchaotic over most of the range $k\in[-12,-1]\cup[1,12]$, and is chaotic in most of the range $k\in[-19.25,-12]\cup[-1,1]\cup[12,19.25]$. The figure also shows that the dynamics of system (4) is symmetric about $k=0$. When k decreases from 25 to 19.30, system (4) firstly enters the quasi-periodic state, and then enters the periodic state again at $k\cong19.75$. Finally, system (4) enters into chaos abruptly at $k\cong19.30$ by a tangent bifurcation. Similarly, when k increases from -25 to -19.30, system (4) firstly enters the quasi-periodic state, then enters the periodic state again at $k\cong-19.75$, and finally enters into chaos abruptly at $k\cong-19.30$ by a tangent bifurcation. Obviously, when $k\neq0$, the introduction of k to the original system will cause the occurrence of hyperchaos and hidden attractors, which provides a new approach for the construction of the complex-variable dynamical system with hyperchaos and hidden attractors.

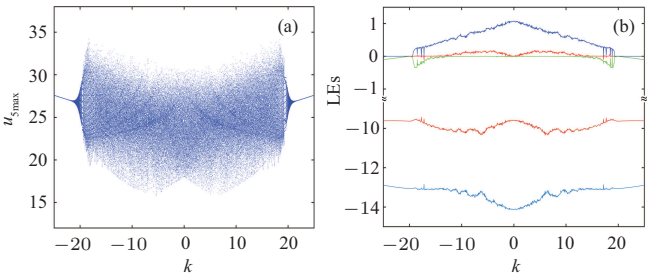


Fig. 6. Dynamics of system (4) with k varying: (a) bifurcation diagram and (b) Lyapunov exponents.

3.3. Extreme multistability and coexisting attractors

For a given parameter set, extreme multistability displays a rich diversity of mutually stable states of a nonlinear dynamical system, and enables the system to provide more flexibility in practical applications. The existence of extreme multistability is discovered in system (4). For example, five coexisting chaotic attractors and five coexisting periodic attractors (limit cycles) of system (4) are shown in Fig. 7, where the blue, red, green, magenta, and cyan attractors are yielded from the initial conditions $(1,1,3,4,5)$, $(1,3,3,4,5)$, $(2,1,3,4,5)$, $(2,3,3,4,5)$, and $(3,5,3,4,5)$, respectively. In fact, for more different initial conditions, more coexisting attractors can be

observed. Moreover, the basin of attraction is generally recognized as an effective approach to disclose the coexistence of attractors. In particular, suppose that the initial values of state variables are chosen as $u_0 = (u_1, u_2, 3, 4, 5)$, then the basins of attraction of system (4) corresponding to different initial conditions at $q = 0.95$, $c = 6.25$, $k = 0$, and $q = 0.95$, $c = 7.50$, $k = 0$ are shown in Fig. 8, where $u_1 \in [-10, 10]$, $u_2 \in [-10, 10]$, and different colors stand for different attractors. Because of the coexistence of infinitely many attractors, system (4) has extreme multistability. It should be noted that the complicated phenomenon is closely related to the rotational symmetry of system (4) about the u_5 axis when $k = 0$. The phenomenon of extreme multistability displays the complicated dynamical behaviors of the fractional-order hyperchaotic complex system, and implies its great engineering application values.

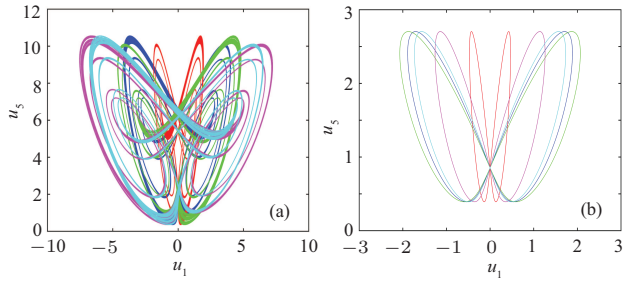


Fig. 7. Coexisting chaotic attractors and coexisting periodic attractors (limit cycles) of system (4) for (a) $q = 0.95$, $c = 6.25$, $k = 0$ (chaotic) and (b) $q = 0.95$, $c = 7.50$, $k = 0$ (periodic).

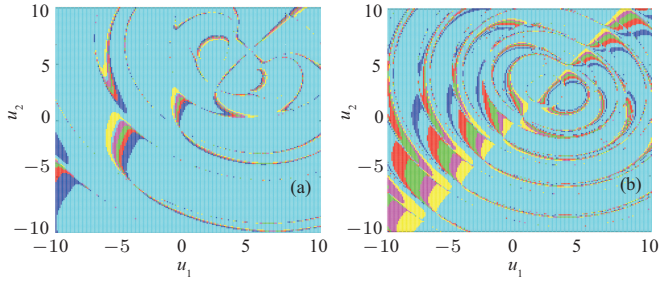


Fig. 8. Basins of attraction of system (4) for (a) $q = 0.95$, $c = 6.25$, $k = 0$ (chaotic) and (b) $q = 0.95$, $c = 7.50$, $k = 0$ (periodic) with the initial condition $u_0 = (u_1, u_2, 3, 4, 5)$.

4. Complex generalized projective synchronization

In this section, the complex generalized projective synchronization of two fractional-order hyperchaotic complex simplified Lorenz systems with different fractional orders is investigated based on the fractional Lyapunov stability theorem.

4.1. Synchronization scheme

The n-dimensional fractional-order complex drive system is depicted as

$$D_{t_0}^{\alpha} x(t) = f(x), \tag{40}$$

and the n-dimensional fractional-order complex response system with synchronization controller is described as

$$D_{t_0}^{\beta} y(t) = g(y) + v(x, y), \tag{41}$$

where $x = (x_1, x_2, \ldots, x_n)^{\mathrm{T}} \in \mathbb{C}^n$ and $y = (y_1, y_2, \cdots, y_n)^{\mathrm{T}} \in \mathbb{C}^n$ are complex state vectors. $f : \mathbb{C}^{n\times 1} \to \mathbb{C}^{n\times 1}$ and $g : \mathbb{C}^{n\times 1} \to \mathbb{C}^{n\times 1}$ are $n \times 1$ complex function vectors. $v(x, y)$ is the synchronization controller, and α, β are the fractional orders of the drive system (40) and the response system (41), respectively. In addition, $\alpha \geq \beta$.

The projective synchronization error $e(t)$ between the drive system (40) and the response system (41) is expressed as

$$e(t) = e^r(t) + \mathrm{j}e^i(t) = y(t) - \Phi x(t), \tag{42}$$

where $\Phi \in \mathbb{C}^{n\times n}$ is an arbitrary complex constant matrix. Therefore, the corresponding error dynamical system is obtained as

$$D_{t_0}^{\alpha} e(t) = D_{t_0}^{\alpha-\beta}(g(y) + v(x, y)) - \Phi f(x). \tag{43}$$

Next, the complex generalized projective synchronization of two fractional-order complex-variable dynamical systems with different fractional orders is defined as follows.

Definition 2 For the drive system (40) and response system (41), if there exists a synchronization controller $v(x, y)$, such that $\lim_{t\to+\infty} \|y(t) - \Phi x(t)\| = 0$, where $\|\cdot\|$ represents the Euclidean norm, then the complex generalized projective synchronization is achieved between the drive system (40) and the response system (41) with different fractional orders.

Lemma 1[42] Let $x(t) \in \mathbb{R}^n$ be a continuous and derivable function, then for all $t \geq t_0$, the following inequality holds

$$\frac{1}{2} D_{t_0}^{q} x^{\mathrm{T}}(t) x(t) \leq x^{\mathrm{T}}(t) D_{t_0}^{q} x(t), \quad \forall q \in (0, 1). \tag{44}$$

Lemma 2 (fractional Lyapunov stability theorem)[43] If there exists a positive definite Lyapunov function $V(x)$ such that $D_{t_0}^{q} V(x) < 0$ for all $t \geq t_0$, then the trivial solution of the fractional-order system $D_{t_0}^{q} x(t) = f(x)$ is asymptotically stable.

Theorem 1 For the given complex constant matrix Φ as well as the initial conditions $x(0)$ and $y(0)$, if the synchronization controller $v(x, y)$ is designed as

$$v(x, y) = -g(y) + J_{t_0}^{\alpha-\beta}(\Phi f(x) + Pe), \tag{45}$$

where $J_{t_0}^{\alpha-\beta}$ is the Riemann–Liouville fractional-order integral operator of order $\alpha - \beta$, and $P = \mathrm{diag}[p_1, p_2, \cdots, p_n]$ is the feedback gain matrix, whose diagonal elements are negative real numbers, then the complex generalized projective synchronization is achieved between the drive system (40) and the response system (41) with different fractional orders.

Proof Substituting Eq. (45) into Eq. (43), then the error

dynamical system is

$$D_{t_0}^{\alpha} e(t) = Pe(t). \tag{46}$$

We define the Lyapunov function as

$$V(t) = \frac{1}{2}(e^r)^{\mathrm{T}} e^r + \frac{1}{2}(e^i)^{\mathrm{T}} e^i. \tag{47}$$

According to Lemma 1, its time derivative of order α satisfies

$$\begin{aligned} D_{t_0}^{\alpha} V(t) &= \frac{1}{2} D_{t_0}^{\alpha}(e^r)^{\mathrm{T}} e^r + \frac{1}{2} D_{t_0}^{\alpha}(e^i)^{\mathrm{T}} e^i \\ &\le (e^r)^{\mathrm{T}} D_{t_0}^{\alpha} e^r + (e^i)^{\mathrm{T}} D_{t_0}^{\alpha} e^i \\ &= (e^r)^{\mathrm{T}} P e^r + (e^i)^{\mathrm{T}} P e^i < 0. \end{aligned} \tag{48}$$

Obviously, $D_{t_0}^{\alpha} V(t)$ is negative definite, and according to Lemma 2, the error dynamical system (43) is asymptotically stable at the origin, *i.e.*, $\lim_{t\to+\infty} \|e(t)\| = 0$. Therefore, the complex generalized projective synchronization is achieved between the drive system (40) and the response system (41) with different fractional orders. The proof is completed.

4.2. Numerical simulations

For the investigation of the complex generalized projective synchronization of two fractional-order hyperchaotic complex simplified Lorenz systems, the drive system is depicted as

$$\begin{cases} D_{t_0}^{\alpha} x_1 = 10(x_2 - x_1), \\ D_{t_0}^{\alpha} x_2 = (24 - 4c)x_1 + cx_2 - x_1 x_3 + k, \\ D_{t_0}^{\alpha} x_3 = -8/3 x_3 + 1/2(\bar{x}_1 x_2 + x_1 \bar{x}_2), \end{cases} \tag{49}$$

and the response system with synchronization controllers is described as

$$\begin{cases} D_{t_0}^{\beta} y_1 = 10(y_2 - y_1) + v_1, \\ D_{t_0}^{\beta} y_2 = (24 - 4c)y_1 + cy_2 - y_1 y_3 + k + v_2, \\ D_{t_0}^{\beta} y_3 = -8/3 y_3 + 1/2(\bar{y}_1 y_2 + y_1 \bar{y}_2) + v_3, \end{cases} \tag{50}$$

where v_1, v_2, v_3 are the synchronization controllers, and α, β are the fractional orders of the drive system (49) and the response system (50), respectively. If the complex constant matrix Φ is selected as

$$\Phi = \begin{bmatrix} 0 & 1+2\mathrm{j} & 0 \\ 3+4\mathrm{j} & 0 & 0 \\ 0 & 0 & 5 \end{bmatrix}, \tag{51}$$

then the errors between the drive system (49) and the response system (50) are expressed as

$$\begin{cases} e_1 = y_1 - (1+2\mathrm{j})x_2, \\ e_2 = y_2 - (3+4\mathrm{j})x_1, \\ e_3 = y_3 - 5x_3. \end{cases} \tag{52}$$

Therefore, the error dynamical system is obtained as

$$\begin{cases} D_{t_0}^{\alpha} e_1 = D_{t_0}^{\alpha-\beta}[10(y_2 - y_1) + v_1] - (1+2\mathrm{j})[(24-4c)x_1 + cx_2 - x_1 x_3 + k], \\ D_{t_0}^{\alpha} e_2 = D_{t_0}^{\alpha-\beta}[(24-4c)y_1 + cy_2 - y_1 y_3 + k + v_2] - (30+40\mathrm{j})(x_2 - x_1), \\ D_{t_0}^{\alpha} e_3 = D_{t_0}^{\alpha-\beta}[-8/3 y_3 + 1/2(\bar{y}_1 y_2 + y_1 \bar{y}_2) + v_3] + 40/3 x_3 - 5/2(\bar{x}_1 x_2 + x_1 \bar{x}_2). \end{cases} \tag{53}$$

According to Theorem 1, if the synchronization controllers v_1, v_2, v_3 are designed as

$$\begin{cases} v_1 = 10(y_1 - y_2) + J_{t_0}^{\alpha-\beta}\{(1+2\mathrm{j})[(24-4c)x_1 + cx_2 - x_1 x_3 + k] + p_1 e_1\}, \\ v_2 = (4c-24)y_1 - cy_2 + y_1 y_3 - k + J_{t_0}^{\alpha-\beta}[(30+40\mathrm{j})(x_2 - x_1) + p_2 e_2], \\ v_3 = 8/3 y_3 - 1/2(\bar{y}_1 y_2 + y_1 \bar{y}_2) + J_{t_0}^{\alpha-\beta}[-40/3 x_3 + 5/2(\bar{x}_1 x_2 + x_1 \bar{x}_2) + p_3 e_3], \end{cases} \tag{54}$$

then the complex generalized projective synchronization is achieved between the drive system (49) and the response system (50) with different fractional orders.

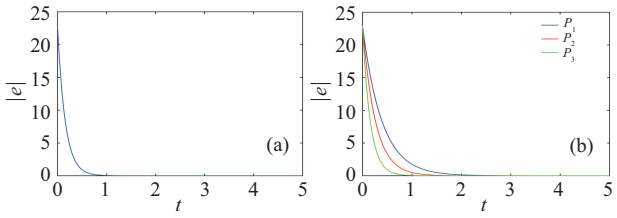


Fig. 9. Time evolutions of the synchronization error (a) $|e|$ *versus* t and (b) $|e|$ *versus* t with different feedback gain matrices.

In the numerical simulations, the system parameters are fixed as $c = 2.5$, $k = 3.5$, and the fractional orders of the drive system (49) and the response system (50) are given as $\alpha = 0.95$, and $\beta = 0.90$, respectively. Moreover, the initial values of state variables are randomly chosen as $x(0) = (1+2\mathrm{j}, 3+4\mathrm{j}, 5)$, and $y(0) = (6+7\mathrm{j}, 8+9\mathrm{j}, 10)$. The feedback gain matrix P is selected as $P = \mathrm{diag}[-5, -5, -5]$. Time evolution of the synchronization error is plotted in Fig. 9(a), where $|e| = \sqrt{|e_1|^2 + |e_2|^2 + |e_3|^2}$. The figure shows that the complex generalized projective synchronization is achieved between the drive system (49) and the response system (50) with different fractional orders. In addition, it is found that the feedback gain matrix P plays an important role in the proposed synchronization scheme. To illustrate the influence of the feedback gain matrix P, time evolutions of the synchronization error for different feedback gain matrices are plotted in Fig. 9(b), where $P1 = \mathrm{diag}[-2, -2, -2]$, $P2 = \mathrm{diag}[-3, -3, -3]$, and $P3 = \mathrm{diag}[-5, -5, -5]$. The figure illustrates that the stronger the selected feedback gain matrix, the faster the complex gen-

eralized projective synchronization is achieved between the drive system (49) and the response system (50) with different fractional orders. The numerical simulations verify and demonstrate the correctness of the theoretical results.

5. Conclusions

In this paper, a novel fractional-order hyperchaotic complex system is constructed by introducing the Caputo fractional-order derivative operator and a constant term to the complex simplified Lorenz system. The fractional-order hyperchaotic complex simplified Lorenz system is solved by the Adomian decomposition method. The dynamical characteristics of the proposed system are analyzed in detail. The research results show that it has different numbers of equilibria for different ranges of parameters. Particularly, the proposed system has the property of extreme multistability, and exhibits four different types of hidden attractors. In addition, the complex generalized projective synchronization is implemented between two fractional-order hyperchaotic complex simplified Lorenz systems with different fractional orders. The fractional Lyapunov stability theorem is applied to design the synchronization controllers, and the correctness of the theoretical results is illustrated by the numerical simulations. Future work will focus on the applications of the fractional-order hyperchaotic complex simplified Lorenz system in engineering fields, such as secure communication and image encryption.

Acknowledgments

Project supported by the National Natural Science Foundation of China (Grant Nos. 62071496, 61901530, and 62061008) and the Innovation Project of Graduate of Central South University (Grant No. 2022zzts0681).

References

[1] Sun H H, Abdelwahab A and Onaral B 1984 *IEEE Trans. Automat. Control* **29** 441
[2] Diethelm K, Ford N J and Freed A D 2002 *Nonlinear Dyn.* **29** 3
[3] G. Adomian 1984 *J. Math. Anal. Appl.* **102** 420
[4] Zhang H Y, Sun K H and He S B 2021 *Nonlinear Dyn.* **106** 1027
[5] Peng D, Sun K H and Alamodi A O A 2019 *Int. J. Mod. Phys. B* **33** 1950031
[6] Wang H H, Zhan D L, Wu X M and He S B 2022 *Eur. Phys. J. Spec. Top.* **231** 2467
[7] Li X J, Mou J, Banerjee S, Wang Z S and Cao Y H 2022 *Chaos, Solitons and Fractals* **159** 112133
[8] Ye X L, Wang X Y, Mou J, Yan X P and Xian Y J 2018 *Eur. Phys. J. Plus* **133** 516
[9] Ma C G, Mou J, Yang F F and Yan H Z 2020 *Eur. Phys. J. Plus* **135** 100
[10] Liu T M, Yan H Z, Banerjee S and Mou J 2021 *Chaos, Solitons and Fractals* **145** 110791
[11] Fowler A C, Gibbon J D and McGuinness M J 1982 *Physica D* **4** 139
[12] Mahmoud G M, Bountis T and Mahmoud E E 2007 *Int. J. Bifurcat. Chaos* **17** 4295
[13] Mahmoud G M, Ahmed M E and Mahmoud E E 2008 *Int. J. Mod. Phys. C* **19** 1477
[14] Mahmoud G M, Mahmoud E E and Ahmed M E 2009 *Nonlinear Dyn.* **58** 725
[15] Luo C and Wang X Y 2013 *Nonlinear Dyn.* **71** 241
[16] Luo C and Wang X Y 2013 *Int. J. Mod. Phys. C* **24** 1350025
[17] Yang F F, Mou J, Liu J, Ma C G and Yan H Z 2020 *Signal Process.* **169** 107373
[18] Pecora L M and Carroll T L 1990 *Phys. Rev. Lett.* **64** 821
[19] Mahmoud G M and Mahmoud E E 2012 *Nonlinear Dyn.* **67** 1613
[20] Mahmoud G M and Mahmoud E E 2010 *Nonlinear Dyn.* **62** 875
[21] Liu D F, Wu Z Y and Ye Q L 2014 *Nonlinear Dyn.* **75** 209
[22] Luo C and Wang X Y 2013 *J. Franklin Inst.* **350** 2646
[23] Sun J W, Cui G Z, Wang Y F and Shen Y 2015 *Nonlinear Dyn.* **79** 953
[24] Liu J, Chen G R and Zhao X 2021 *Fractals* **29** 2150081
[25] He S B, Sun K H, Wang H H, Mei X Y and Sun Y F 2018 *Nonlinear Dyn.* **92** 85
[26] Hens C, Dana S K and Feudel U 2015 *Chaos* **25** 053112
[27] Bao B C, Xu Q, Bao H and Chen M 2016 *Electron Lett.* **52** 1008
[28] Bao B C, Jiang T, Wang G Y, Jin P P, Bao H and Chen M 2017 *Nonlinear Dyn.* **89** 1157
[29] Lai Q, Kuate P D K, Liu F and Iu H H C 2020 *IEEE Trans. Circuits Syst. II Express Briefs* **67** 1129
[30] Bao H, Liu W B and Chen M 2019 *Nonlinear Dyn.* **96** 1879
[31] Chang H, Li Y X, Yuan F and Chen G R 2019 *Int. J. Bifurcat. Chaos* **29** 1950086
[32] Yuan F, Wang G Y and Wang X W 2016 *Chaos* **26** 073107
[33] Dudkowski D, Jafari S, Kapitaniak T, Kuznetsov N V, Leonov G A and Prasad A 2016 *Phys. Rep.* **637** 1
[34] Wei Z C 2011 *Phys. Lett. A* **376** 102
[35] Pham V T, Volos C, Jafari S, Wei Z C and Wang X 2014 *Int. J. Bifurcat. Chaos* **24** 1450073
[36] Lai Q, Wan Z Q and Kuate P D K 2020 *Electron Lett.* **56** 1044
[37] Sun K H and Sprott J C 2009 *Int. J. Bifurcat. Chaos* **19** 1357
[38] Jin M X, Sun K H and Wang H H 2021 *Nonlinear Dyn.* **106** 2667
[39] Petras I 2010 *IEEE Trans. Circuits Syst. II Express Briefs* **57** 975
[40] Sun K H, Liu X and Zhu C X 2010 *Chin. Phys. B* **19** 110510
[41] Von-Bremen H F, Udwadia F E and Proskurowski W 1997 *Physica D* **101** 1
[42] Aguila-Camacho N, Duarte-Mermoud M A and Gallegos J A 2014 *Commun. Nonlinear Sci. Numer. Simul.* **19** 2951
[43] Chen D Y, Zhang R F, Liu X Z and Ma X Y 2014 *Commun. Nonlinear Sci. Numer. Simul.* **19** 4105